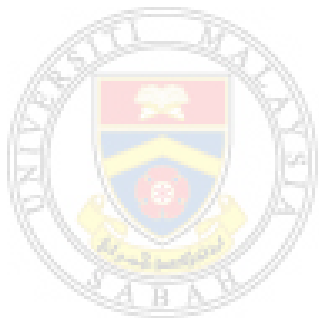


**SYNTHESISATION OF DIVERSE AND
PHOTOREALISTIC LUNG IMAGES FOR LUNG
DISEASES RECOGNITION USING DEEP
LEARNING TECHNIQUES**

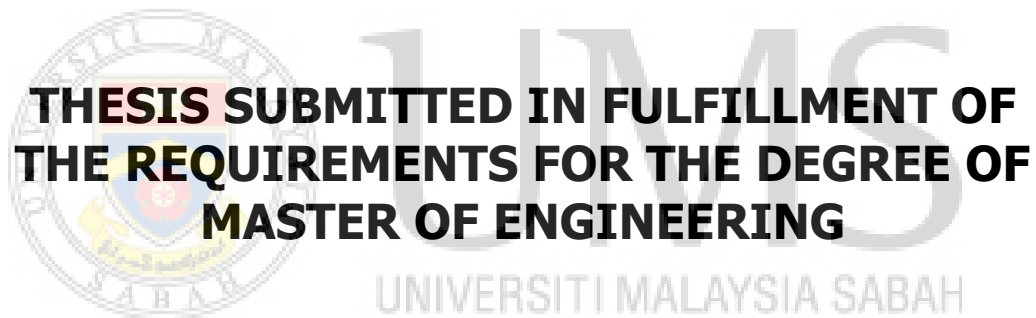


LEE KIN WAI
UMS
UNIVERSITI MALAYSIA SABAH

**FACULTY OF ENGINEERING
UNIVERSITI MALAYSIA SABAH
2023**

**SYNTHESISATION OF DIVERSE AND
PHOTOREALISTIC LUNG IMAGES FOR LUNG
DISEASES RECOGNITION USING DEEP
LEARNING TECHNIQUES**

LEE KIN WAI



**FACULTY OF ENGINEERING
UNIVERSITI MALAYSIA SABAH
2023**

UNIVERSITI MALAYSIA SABAH
BORANG PENGESAHAN STATUS TESIS

JUDUL : **SYNTHESISATION OF DIVERSE AND PHOTOREALISTIC LUNG IMAGES FOR LUNG DISEASES RECOGNITION USING DEEP LEARNING TECHNIQUES**

IJAZAH : **SARJANA KEJURUTERAAN**

BIDANG : **KEJURUTERAAN KOMPUTER**

Saya **LEE KIN WAI**, Sesi **2020-2023**, mengaku membenarkan tesis Sarjana ini disimpan di Perpustakaan Universiti Malaysia Sabah dengan syarat-syarat kegunaan seperti berikut:-

1. Tesis ini adalah hak milik Universiti Malaysia Sabah
2. Perpustakaan Universiti Malaysia Sabah dibenarkan membuat salinan untuk tujuan pengajian sahaja.
3. Perpustakaan dibenarkan membuat salinan tesis ini sebagai bahan pertukaran antara institusi pengajian tinggi.
4. Sila tandakan (/):

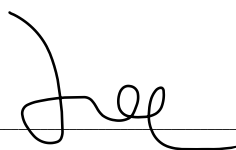
SULIT

(Mengandungi maklumat yang berdarjah keselamatan atau kepentingan Malaysia seperti yang termaktub di dalam AKTA RAHSIA 1972)


TERHAD

(Mengandungi maklumat TERHAD yang telah ditentukan oleh organisasi/badan di mana penyelidikan dijalankan)

TIDAK TERHAD



LEE KIN WAI
MK2011034T

Disahkan Oleh,

ANITA BINTI ARSAD
PUSTAKAWAN KANAN
UNIVERSITI MALAYSIA SABAH

(Tandatangan Pustakawan)

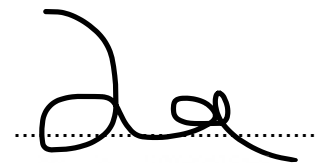
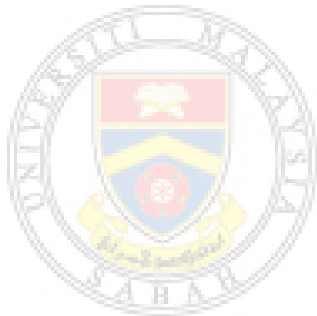
Tarikh : 17 Februari 2023

(Assoc Prof. Dr. Renee Chin Ka Yin)
Penyelia

DECLARATION

I hereby declare that this project entitled "Synthesis of Diverse and Photorealistic Lung Images for Lung Diseases Recognition using Deep Learning Techniques", submitted to Universiti Malaysia Sabah, is an original work done by me under the guidance of supervisor AP. Dr. Renee Chin, and it is submitted as the fulfilment of the requirement for the degree of Master of Computer Engineering, which has not been submitted to any other university for any degree. I also certify that the work described here is entirely mine, except for quotations and summaries sources which have been acknowledged. This thesis may be made available within the university library and may be photocopied or loaded to other libraries for the purposes of consultation.

24 November 2022

A handwritten signature in black ink, appearing to read "Lee Kin Wai", written over a dotted line.

Lee Kin Wai
MK2011034T

UMMS
UNIVERSITI MALAYSIA SABAH

CERTIFICATION

NAME : LEE KIN WAI
MATRIC NO. : MK2011034T
TITLE : SYNTHESISATION OF DIVERSE AND
PHOTOREALISITC LUNG IMAGES FOR LUNG
DISEASES RECOGNITION USING DEEP LEARNING
TECHNIQUES
DEGREE : MASTER OF ENGINEERING
PROGRAM : COMPUTER ENGINEERING
VIVA DATE : 24 NOVEMBER 2022

CERTIFIED BY;


SUPERVISOR
Assoc Prof. Dr. Renee Chin Ka Yin

Signature


UNIVERSITI MALAYSIA SABAH

ACKNOWLEDGEMENT

Firstly, I would like to express my sincere gratitude to my project supervisor AP. Dr. Renee Chin for the continuous support of my master's degree research project and related research work, for her patience and inspiring advice. Her guidance provided the truthful direction throughout accomplishment of the project.

Besides, my honest thanks to Universiti Malaysia Sabah for the financial support for my project. I would like to express my appreciation to Dr. Teh Yong Guang from the Faculty of Medicine and Health Sciences, Universiti Malaysia Sabah for this contribution in the examination of the synthetic COVID-19 CT images.

Last but not least, family is indeed my emotional support. Whenever things turned out to be depressing, my parents are always be there to ease the pain and helps me to get comfortable in all stressful situation.

Lee Kin Wai
24 November 2022



UMMS
UNIVERSITI MALAYSIA SABAH

ABSTRACT

Deep Learning (DL) techniques leverage the rich data diversity in the modern era of Big Data, allowing possibilities of achieving human-level performances in many real-world problems. However, newly emerged problems such as the ongoing COVID-19 pandemic have underscored the challenge of acquiring a larger corpus of data during the early stages of the pandemic due to the availability of samples, data protection policies, labour, and facility resources. Furthermore, the effectiveness of existing DL models that are trained on older datasets might be vulnerable to the continuous emergence of COVID-19 variants that may potentially result in distribution shifts. This research introduces a data synthesis framework named stacked residual dropout generative adversarial network (sRD-GAN), which alleviates the problem of data paucity by generating synthetic lung medical images that contain precise radiographic feature annotations. The underlying design of sRD-GAN is an Image-to-Image translation setting that facilitates instance-level diversity via the latent space stochasticity induced by the novel stacked residual dropout (sRD) regularization. To this end, experiments show that sRD-GAN achieved perceptually significant structural dissimilarities of the ground glass opacities (GGO) from diverse COVID-19 CT images without disentangling the content-style attributes of the images as in conventional multimodal image translation techniques. Since the sRD regularization is a strategic incorporation of the conventional dropout regularization, which can be generalized across neural network models, the sRD regularization can be easily incorporated into existing image synthesizer models without modifying the original setup of these models. In addition, a new training loss function known as adaptive pixel consistency loss is proposed for effective noise reduction by encouraging structural similarity of the invariance features of the images from both domains. Quantitative results show that the synthetic COVID-19 CT images achieve a promising Fréchet Inception Distance (FID) of 58.68, which is superior to existing GAN baselines such as GAN (157.18), CycleGAN (115.14), and One-to-one CycleGAN (94.11). Visual examination of the synthetic images also indicates excellent perceptual image quality and realism, where synthetic radiographic features of GGO achieve consistency with real COVID-19 CT images examined by an experienced radiologist. Furthermore, the effectiveness of the proposed sRD-GAN is also validated on Community-Acquired Pneumonia (CAP) CT images and COVID-19 X-Ray images, which achieved comparable performances with COVID-19 CT images. This suggests that the proposed method can be easily extended to other similar applications. Lastly, the sRD-GAN is applied to the problem of COVID-19 disease recognition in the form of dynamic data augmentation. Empirical results suggest that synthetic images can approximate real data distribution for model training purposes. Specifically, the VGG19 models achieve the highest accuracy score at 97.54% on the test set when training with fully synthetic COVID-19 CT images in 3000-images dataset size, contributing to a 12.95% accuracy improvement from training with only real image data.

ABSTRAK

SINTESIS IMEJ PARU-PARU YANG KEPELBAGAIAN DAN FOTOREALISTIK UNTUK PENGECAMAN PENYAKIT PARU PARU-PARU MENGGUNAKAN TEKNIK PEMBELAJARAN MENDALAM

Teknik Pembelajaran Dalam (DL) memanfaatkan kepelbagaian data yang kaya dalam era moden Data Besar, membolehkan kemungkinan mencapai prestasi peringkat manusia dalam banyak masalah dunia sebenar. Namun, masalah yang baru timbul seperti pandemik COVID-19 yang berterusan telah menggariskan cabaran untuk memperoleh korpus data yang lebih besar semasa peringkat awal wabak disebabkan oleh ketersediaan sampel, dasar perlindungan data, tenaga buruh, dan sumber kemudahan. Selain itu, keberkesanan model DL sedia ada yang dilatih pada set data lama mungkin terdedah kepada kemunculan berterusan varian COVID-19 yang berpotensi mengakibatkan anjakan pengedaran. Penyelidikan ini memperkenalkan rangka kerja sintesis data yang dinamakan rangkaian adversarial generatif stacked residual dropout (sRD-GAN), yang dapat menghasilkan imej perubahan paru-paru sintetik yang mengandungi anotasi ciri radiografi yang tepat. Reka bentuk asas sRD-GAN ialah Imej-ke-Imej melalui stokastik ruang terpendam yang disebabkan oleh regularisasi stacked residual dropout (sRD). Untuk tujuan ini, eksperimen menunjukkan bahawa sRD-GAN mencapai ketidaksamaan struktur yang ketara secara persepsi bagi kelegapan kaca tanah (GGO) daripada imej CT COVID-19 yang pelbagai tanpa memerlukan merungkai atribut style-content imej seperti dalam teknik terjemahan imej multimodal konvensional. Memandangkan regularization sRD ialah penggabungan strategik regularization dropout konvensional, regularization sRD boleh dimasukkan ke dalam model sintesis imej sedia ada tanpa mengubah suai persediaan asal model ini. Selain itu, fungsi latihan baharu yang dikenali sebagai kehilangan ketekalan piksel adaptif dicadangkan untuk pengurangan hingar yang berkesan dengan menggalakkan persamaan struktur ciri invarian imej daripada kedua-dua domain. Keputusan kuantitatif menunjukkan bahawa imej CT COVID-19 sintetik mencapai Fréchet Inception Distance (FID) yang menjanjikan sebanyak 58.68, yang lebih baik daripada garis dasar GAN sedia ada seperti GAN (157.18), CycleGAN (115.14) dan One-to-one CycleGAN (94.11). Pemeriksaan visual imej sintetik juga menunjukkan kualiti imej persepsi yang sangat baik dan realisme, di mana ciri radiografi sintetik GGO mencapai konsistensi dengan imej CT COVID-19 sebenar yang diperiksa oleh ahli radiologi berpengalaman. Selain itu, keberkesanan sRD-GAN yang dicadangkan juga disahkan pada imej CT Pneumonia Diperolehi Masyarakat (CAP) dan imej X-Ray COVID-19, yang mencapai prestasi yang setanding dengan imej CT COVID-19. Ini menunjukkan bahawa kaedah yang dicadangkan boleh diperluaskan dengan mudah kepada kes lain yang serupa. Akhir sekali, sRD-GAN digunakan dalam masalah pengecaman penyakit COVID-19 dalam bentuk penambahan data dinamik. Keputusan empirikal menunjukkan bahawa imej sintetik boleh menganggarkan pengedaran data sebenar untuk tujuan latihan model. Khususnya, model VGG19 mencapai skor ketepatan tertinggi pada 97.54% pada set ujian apabila berlatih dengan imej CT COVID-19 sintetik sepenuhnya dalam saiz set data 3000 imej, yang menyumbang kepada peningkatan ketepatan 12.95% daripada latihan dengan hanya data imej sebenar.

LIST OF CONTENTS

	Page
TITLE	i
DECLARATION	ii
CERTIFICATION	iii
ACKNOWLEDGEMENT	iv
ABSTRACT	v
<i>ABSTRAK</i>	vi
LIST OF CONTENTS	vii
LIST OF TABLES	xii
LIST OF FIGURES	xiii
LIST OF SYMBOLS	xvii
LIST OF ABBREVIATIONS	xix
LIST OF APPENDICES	xxi
CHAPTER 1 : INTRODUCTION	
1.1 Research Background	1
1.1.1 Data Augmentation as a Solution to Data Paucity	3
1.1.2 Generative Modelling and Generative Data Augmentation	4
1.2 Problem Statement	6
1.3 Aim and Objective	7
1.4 Hypothesis	8
1.5 Scope of Study	8
1.6 Thesis Structure	10
CHAPTER 2 : LITERATURE REVIEW	
2.1 Chapter Overview	12
2.2 Radiological examination of COVID-19	12

2.2.1	Role of Radiology in COVID-19 Diagnosis	13
2.2.2	Effectiveness of Imaging Modalities in COVID-19 Diagnosis	14
2.3	Integration of Artificial Intelligence in COVID-19 Diagnosis	15
2.3.1	Challenges of Medical Imaging in COVID-19 Diagnosis	16
2.3.2	COVID-19 Diagnosis with Machine Learning Techniques	17
2.3.3	More Discriminative COVID-19 Classification	19
2.3.4	Techniques to improve the performance of the Detection and Classification Models	20
2.4	Data Augmentation as a Solution for Data Paucity	22
2.4.1	Data Augmentation Techniques	22
2.4.2	Generative Data Augmentation in COVID-19 Detection and Classification	25
2.5	Generative Adversarial Networks (GANs)	26
2.5.1	Advancement of GANs	28
2.5.2	Application of GANs in Medical Images	31
2.5.3	Improved Image Quality with Unpaired Image-to-Image Translation	36
2.6	Diverse Image Synthesis	41
2.6.1	Introduction to multimodality and disentangled learning	41
2.6.2	Regularization Techniques to Facilitate Latent Space Stochasticity	44
2.6.3	Fine-grained Feature Translation	46
2.7	Chapter Summary	47
CHAPTER 3 : METHODOLOGY		
3.1	Chapter Overview	48
3.2	Problem Setting and Assumption	48
3.3	Stacked Residual Dropout (sRD) Mechanism	51
3.3.1	Building Block of Residual-Convolution Layers	51
3.3.2	Two-Mode Mechanism	53
3.4	Stacked Residual Dropout Generative Adversarial Network (sRD-GAN)	56
3.4.1	Overview of sRD-GAN	56
3.4.2	Models	58
3.4.3	Loss Functions	59

3.5	Datasets	62
3.6	Performance Evaluation	63
3.6.1	Radiologist Examination	64
3.6.2	Learned Perceptual Image Patch Similarity (LPIPS)	64
3.6.3	Fréchet Inception Distance (FID)	64
3.6.4	Visualization tools	65
3.6.5	Other Metrics	66
3.7	Preliminary Experiment and Hyperparameter Setup	66
3.7.1	Preliminary Experiment Setup	67
3.7.2	Preliminary Results and Findings	68
3.7.3	GANs Training Graph	72
3.7.4	Hyperparameter Tuning	75
3.8	Software and Hardware resources	76
3.9	Chapter Summary	77

CHAPTER 4 : EXPERIMENT AND RESULT

4.1	Chapter Overview	78
4.2	Experiment 1: sRD-GAN in Training Mode	79
4.2.1	Experiment Implementation	79
4.2.2	Result and Analysis	80
4.3	Experiment 2: Amplification Latent Space Stochasticity in Inference Mode	85
4.3.1	Experiment Implementation	86
4.3.2	Result Interpretation	86
4.4	Experiment 3: Impact of Different Dropout rates on the Synthetic Images	94
4.4.1	Experiment Implementation	94
4.4.2	Result Interpretation	95
4.5	Experiment 4: Single RD-activation at Different Latent Dimensionality	100
4.5.1	Experiment Implementation	101
4.5.2	Result Interpretation	102
4.6	Experiment 5: Multiple RD-activations	104
4.6.1	Experiment Implementation	105

4.6.2	Result Interpretation	106
4.7	Experiment 6: Effectiveness of pixel-consistency constraint for Effective Noise Reduction	109
4.7.1	Experiment Implementation	109
4.7.2	Result Interpretation	110
4.7.3	Validation of Perceptual Realism of the Synthetic Images	115
4.8	Chapter Summary	120

CHAPTER 5 : PERFORMANCE BENCHMARKING, GENERALIZATION, AND FAILURE ANALYSIS

5.1	Chapter Overview	122
5.2	Performance Benchmarking with Existing GANs	122
5.2.1	Setup	123
5.2.2	Result Interpretation	124
5.3	Integration of sRD Regularization on Conventional GANs	127
5.3.1	Setup	128
5.3.2	Result Interpretation	128
5.4	Adaptation of sRD-GAN in External Clinical Cases	131
5.4.1	Setup	132
5.4.2	Result Interpretation	132
5.4.3	Important Findings	135
5.5	Failure Analysis 1: Failure of Image Translation	136
5.5.1	Unpredictable Transfer of Synthetic Features	136
5.5.2	Image Synthesis from Problematic Datasets	140
5.6	Failure Analysis 2: Inaccurate Quantitative Measurement	142
5.7	Chapter Summary	146

CHAPTER 6 : SIGNIFICANCE OF SYNTHETIC COVID-19 CT IMAGES ON COVID-19 DETECTION

6.1	Chapter Overview	147
6.2	COVID-19 Detection with Data Augmentation	147
6.2.1	Dataset Structures	148
6.2.2	Data Augmentation Techniques	149
6.2.3	Neural Network Architecture	150

6.2.4	Experiment Implementation	150
6.2.5	Performance Metrics	151
6.3	Result and Analysis	152
6.3.1	Effectiveness of Dataset Expansion Via Data Augmentation	152
6.3.2	Impact of the DNN architectures on the model's performance	156
6.3.3	Performance Validation using Segregated Datasets	159
6.4	Gradient-Class Activation Map (GradCAM) Analysis	164
6.4.1	False Positive Predictions	164
6.4.2	Failure detection of GGO features	167
6.4.3	Enhanced Attention Annotation with Synthetic Images	169
6.5	Chapter Summary	170

CHAPTER 7 : CONCLUSION

7.1	Chapter Overview	172
7.2	Research Summary	172
7.3	Limitations and Future Work	175
7.4	Prospective Applications	176
	REFERENCES	177
	APPENDICES	188

LIST OF TABLES

	Page
Table 4.1 : Performance metrics of the sRD-GAN trained with different numbers of RD blocks in training and inference mode	81
Table 4.2 : Performance of the sRD-GAN trained with different numbers of RD blocks in training and inference mode	87
Table 5.1 : Configuration of the GANs for performance benchmarking	124
Table 5.2 : Performance metrics of the images generated by the GAN algorithms	124
Table 6.1 : Dataset structures from real and synthetic images	148



UMS
UNIVERSITI MALAYSIA SABAH

LIST OF FIGURES

	Page
Figure 1.1 : (a) Image of zebras and transformed into colours of horses, (b) Image of oranges and transformed into	5
Figure 2.1 : Illustration of the discriminator and the generator model from the perspective of data space	27
Figure 2.2 : Each output vector represents 70 x 70 patches of the input image for 70 x 70 PatchGAN architecture	34
Figure 2.3 : Synthetic COVID-19 CT images generated by the I2I algorithm using cGAN	35
Figure 2.4 : Illustration of the latent spaces and mapping designs of CycleGAN and UNIT architectures	37
Figure 2.5 : The content and style attributes are disentangled into separated spaces in (a) and generates diverse output from the encoded style attributions in (b)	42
Figure 3.1 : A single residual block of the image transformation network	52
Figure 3.2 : Overview of the sRD Mechanism in two different modes	55
Figure 3.3 : Overview of sRD-GAN framework	57
Figure 3.4 : synthetic COVID-19 CT images generated from GAN and CycleGAN	68
Figure 3.5 : FID scores of 100 testing images generated from GAN at every 10 th training epoch	70
Figure 3.6 : FID scores of 100 testing images generated from CycleGAN ($\lambda_{id}=0.5$) at every 10 th training epoch	70
Figure 3.7 : LPIPS distance of 100 testing images generated from GAN at every 10 th training epoch	71
Figure 3.8 : LPIPS distance of 100 testing images generated from CycleGAN ($\lambda_{id} =0.5$) at every 10 th training epoch	72
Figure 3.9 : Learning Curve of GAN for 100 th epoch	73
Figure 3.10 : Learning Curve of the Generators of the CycleGAN ($\lambda_{id}=0.5$) for 100 epoch	74
Figure 3.11 : Learning Curve of the Discriminators of the CycleGAN ($\lambda_{id}=0.5$) for 100 epochs	74
Figure 4.1 : Configuration of the six variations of sRD mechanism in training mode	79

Figure 4.2	: Synthetic images generated from the sRD-GAN trained with different number of RD blocks in training mode	82
Figure 4.3	: Image difference between a reference output and second output generated from the same model for different number of RD blocks in training mode	83
Figure 4.4	: Images generated from the test set at different training	84
Figure 4.5	: Comparison of LPIPS distance of the images generated by the sRD-GAN in training and inference modes	87
Figure 4.6	: Synthetic images generated from the sRD-GANs trained with different number of RD blocks in inference mode	89
Figure 4.7	: Comparison of FID score of the images generated by the sRD-GAN in training and inference modes	90
Figure 4.8	: Comparison between the outputs generated from sRD-GAN trained with 24 different number of RD blocks in training and inference mode	93
Figure 4.9	: Configurations of nine variations of sRD mechanism with different residual dropout rate in inference mode	95
Figure 4.10	: Comparison of the synthetic images generated from normal dropout rate (0.5) and reduced dropout rate (0.2) of the three middle RD blocks of the image transformation network	96
Figure 4.11	: LPIPS distance of the synthetic images generated with different dropout rate for the first three RD-block	97
Figure 4.12	: FID score of the synthetic images generated with different dropout rate for the first three RD-block	98
Figure 4.13	: Output images generated by the sRD-GAN with different dropout rate in the inference mode	99
Figure 4.14	: Diverse outputs generated from the sRD-GAN trained with the light residual dropout setting and a 0.2 dropout rate in the inference mode	100
Figure 4.15	: Configurations of nine variations of sRD mechanism with different order of single RD-activation in inference mode	101
Figure 4.16	: LPIPS distance of the synthetic images generated with single RD-activation at different orders of residual blocks	102
Figure 4.17	: FID score of the synthetic images generated with single RD-activation at different orders of residual blocks	103
Figure 4.18	: Synthetic images generated by the sRD-GAN with a single RD activation at the 1st, 5th, and 9th residual block	104
Figure 4.19	: Configurations of nine variations of sRD mechanism with different number of RD blocks in inference mode	105
Figure 4.20	: LPIPS distance of the synthetic images generated with	106

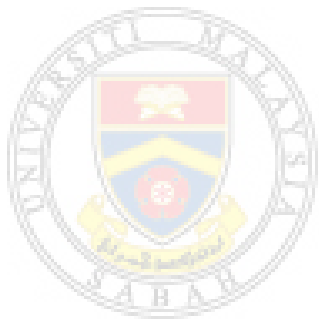
	different RD blocks in inference mode	
Figure 4.21	: FID score of the synthetic images generated with different RD blocks in inference mode	107
Figure 4.22	: Output images generated by the sRD-GAN with increasing number of RD blocks in the inference mode	108
Figure 4.23	: LPIPS distances of the output images generated by different setting of pixel consistency loss in three different GANs	110
Figure 4.24	: FID scores of the output images generated by different setting of pixel consistency loss in three different GANs	111
Figure 4.25	: Synthetic COVID-19 CT images generated GAN baselines with and without adaptive pixel consistency loss	112
Figure 4.26	: Synthetic COVID-19 CT images generated by GAN and CycleGAN with and without pixel consistency loss	114
Figure 4.27	: Confusion matrix of the Visual Turing Test with 30 images of good image synthesis compared to real COVID-19 and non-COVID-19 CT	115
Figure 4.28	: Confusion matrix of the Visual Turing Test with 20 images of bad image synthesis compared to real COVID-19 and non-COVID-19 CT	116
Figure 4.29	: Samples of synthetic COVID-19 CT images examined in the Visual Turing Test	117
Figure 4.30	: GradCAM saliency maps of a pretrained pneumonia detection network on the three categories of images	118
Figure 4.31	: UMAP (n_neighbours = 2, min_dist = 0)	119
Figure 4.32	: UMAP (n_neighbours = 200, min_dist = 0.5)	120
Figure 5.1	: Comparison of the synthetic COVID-19 CT images generated by different GAN baselines	126
Figure 5.2	: Synthetic COVID-19 CT images generated from GAN and three variations of CycleGAN	127
Figure 5.3	: LPIPS distance of the test sets generated from different GANs incorporated with sRD regularization	129
Figure 5.4	: FID Score of the test sets generated from different GANs incorporated with sRD regularization	129
Figure 5.5	: Diverse synthetic COVID-19 CT images generated from different GANs incorporated with sRD mechanism	131
Figure 5.6	: LPIPS distance of the test sets on different clinical cases	133
Figure 5.7	: Synthetic CAP CT images generated by the sRD-GAN in interface mode	134

Figure 5.8	: Synthetic COVID-19 X-ray images generated by the sRD-GAN in interface mode	134
Figure 5.9	: FID score of the test sets on different clinical case	135
Figure 5.10	: Synthetic COVID-19 CT images generated at different training epochs	138
Figure 5.11	: Samples COVID-19 CT images grouped based on the significance of the synthetic features of GGO	139
Figure 5.12	: Synthetic samples generated by the three sRD-GANs that are trained separately	140
Figure 5.13	: Synthetic COVID-19 CT images generated from MosMed Dataset	141
Figure 5.14	: Synthetic COVID-19 CT images generated from a unnamed dataset from Negin Medical Centre of Iran	141
Figure 5.15	: Histogram of the mean pixel values of three different tests sets from various sources	142
Figure 5.16	: Synthetic COVID-19 CT images with varying conditions and their corresponding performance metrics	144
Figure 5.17	: Examples of the style-artifacts observed from the synthetic COVID-19 CT images	145
Figure 6.1	: Samples of augmented image with random rotation and Noise injection	149
Figure 6.2	: Accuracy of the CNNs trained with different number of images and dataset structures	153
Figure 6.3	: Accuracy of the VGG16s trained with different number of images and dataset structures	154
Figure 6.4	: Accuracy of the VGG19s trained with different number of images and dataset structures	155
Figure 6.5	: Accuracy of the DNNs trained with 2000-image datase	157
Figure 6.6	: Accuracy of the DNNs trained with 3000-image dataset	157
Figure 6.7	: Performance metrices of different DNNs and number of images evaluated on images from Negin Medical Center	160
Figure 6.8	: Performance metrices of different DNNs and number of images evaluated on MosMed Dataset	162
Figure 6.9	: GradCAM of the Non-COVID-19 CT images by the CNNs trained with different dataset structures and number of images	166
Figure 6.10	: GradCAM of the COVID-19 CT images by the CNNs trained with different dataset structures and number of images	168
Figure 6.11	: Comparison of GradCAM generated by the CNNs trained with basic and generative augmented data	169

LIST OF SYMBOLS

$G()$	-	Generator model
$D()$	-	Discriminator model
z	-	Noise input distribution
E_x	-	Expected value from the real data distribution
f	-	input image for a convolution operation
h	-	convolution kernel
m	-	Row index of the result matrix
n	-	Column index of the result matrix
j	-	Row index of the kernel matrix
k	-	Column index of the kernel matrix
$F()$	-	Reverse generator model of CycleGAN
x	-	Real base image (Real non-COVID-19)
x'	-	Fake base image (Synthetic non-COVID-19)
y	-	Real style image (Real COVID-19)
y'	-	Fake style image (Synthetic COVID-19)
X	-	Real base image domain (Real non-COVID-19)
X'	-	Fake base image domain (Synthetic non-COVID-19)
Y	-	Real style image domain (Real COVID-19)
Y'	-	Fake style image domain (Synthetic COVID-19)
D_x	-	Reverse Discriminator model
D_y	-	Forward discriminator model
T	-	Bound for stability
c	-	Shared content instance
C	-	Shared content latent space
s	-	Discriminative style instance
S	-	Discriminative style latent space
res	-	Single residual-convolution process (sub block)
RES	-	Double residual-convolution process (primary block)
p	-	Dropout variable
L_{GAN}	-	Adversarial loss
L_{pixel}	-	Pixel consistency loss

- L_{cycle} Cycle consistency loss
- L_{id} Identity loss
- $L()$ Final objective function

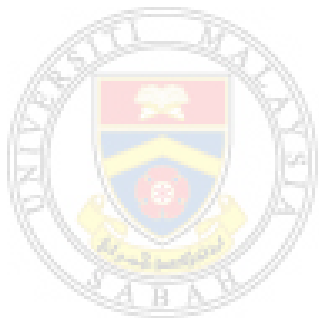


UMMS
UNIVERSITI MALAYSIA SABAH

LIST OF ABBREVIATIONS

AI	-	Artificial Intelligence
ACGAN	-	Auxiliary Classifier Generative Adversarial Network
ANN	-	Artificial Neural Network
CAP	-	Community Acquired Pneumonia
cGAN	-	Conditional
CNN	-	Convolutional Neural Network
COVID-19	-	Coronavirus Disease 2019
CT	-	Computerized Tomography
CycleGAN	-	Cycle Consistency Generative Adversarial Network
DA	-	Data Augmentation
DCGAN	-	Deep Convolutional Generative Adversarial Network
DNN	-	Deep Neural Network
DL	-	Deep Learning
EM	-	Earth-Mover
FCL	-	Fully Connected Layer
FID	-	Fréchet Inception Distance
GAN	-	Generative Adversarial Network
GGO	-	Ground Glass Opacity
GMMs	-	Gaussian Mixture Models
GPU	-	Graphics Processing Unit
GradCAM	-	Gradient Class Activation Map
ILD	-	Interstitial Lung Disease
I2I	-	Image-to-image
IS	-	Inception Score
JSD	-	Jensen-shannon Divergence
KL	-	Kullback-Leibler
LPIPS	-	Learned Perceptual Image patch Similarity
ML	-	Machine Learning
MODE	-	Multi-objective Differential Evolution
MSE	-	Mean Square Error

NST	-	Neural Style Transfer
PCA	-	Principal Component Analysis
PSNR	-	Peak Signal-to-Noise Ratio
RD	-	Residual Dropout
RT-PCR	-	Real-time Polymerase Chain Reaction
SOTA	-	State-of-the-art
sRD	-	Stacked Residual Dropout
SSIM	-	Structural Similarity Index
t-SNE	-	t-distributed Stochastic Neighbouring Embedding
UMAP	-	Uniform Manifold Approximation and Projection
VAE	-	Variational Auto-encoder
WGAN	-	Wasserstein Generative Adversarial Network
WHO	-	World Health Organization



UMS
UNIVERSITI MALAYSIA SABAH

LIST OF APPENDICES

	Page
Appendix A: Description of GAN baselines	188
Appendix B: Performance Metrics for Preliminary Experiment	191
Appendix C: Performance Metrics for Experiment 3 -5	193
Appendix D: Performance Metrics for Experiment 6	194
Appendix E: Synthetic Covid-19 CT Images Generated by sRD-GAN using Test Dataset	195
Appendix F: Covid-19 CT Images for Visual Turing Test	199
Appendix G: Description of Neural Network Architectures for Covid-19 Detection	201
Appendix H: Mean Accuracy Scores of Covid-19 Detection Model in Different Experimental Settings	203
Appendix I: List of Publications	204

CHAPTER 1

INTRODUCTION

1.1 Research Background

The Coronavirus disease 2019 (COVID-19) continues to be devastating since the World Health Organization (WHO) declared the official status of the disease on 11 March 2020 (World Health Organization, 2020). Although the successful administration of COVID-19 vaccination at a global scale has deescalated the disastrous impact of the disease (Feldscher, 2021), the short- and long-term prospects of the disease stay uncertain at present.

The prolonged and terrifying struggle for the past two years has the high vulnerability of humanity against unexpected global-scale catastrophes. The continuous emergence of new COVID-19 variants and the escalation of infection cases, even after the vaccination programs have been established globally, suggest that the COVID-19 pandemic is still far from a complete end. Although there is evidence that shows the effectiveness of the approved vaccines in preventing severe illness due to the virus (Cevik *et al.*, 2021), human beings are still vulnerable to new COVID-19 variants (Person & Steenhuisen, 2021) as there are uncertainties about the mutations and more importantly how they will harm the human body.

While newer generations of vaccines or medications play a crucial role in helping humanity to achieve complete immunity against the coronavirus and its unforeseeable variants, other crucial aspects within the healthcare systems can be